Impact of different El Niño types on the El Niño/IOD relationship

Article

Accepted Version

Impact of different El Niño types on the El Niño/IOD relationship

Wenjun Zhang[1], Yalan Wang[1], Fei-Fei Jin[2], Malte F. Stuecker[2], Andrew G.Turner[3]
[1] Collaborative Innovation Center on Forecast and Evaluation of Meteorological Disasters, KLME, Nanjing University of Information Science and Technology, Nanjing 210044, China
[2]Department of Atmospheric Sciences, SOEST, University of Hawaii, HI 96822, USA
[3]NCAS-Climate and Department of Meteorology, University of Reading, Reading RG6 6BB, UK

Abstract Previous studies reported that positive phases of the Indian Ocean Dipole (IOD) tend to accompany El Niño during boreal autumn. Here we show that the El Niño/IOD relationship can be better understood when considering the two different El Niño flavors. Eastern-Pacific (EP) El Niño events exhibit a strong correlation with the IOD dependent on their magnitude. In contrast, the relationship between Central-Pacific (CP) El Niño events and the IOD depends mainly on the zonal location of the sea surface temperature anomalies rather than their magnitude. CP El Niño events lying further west than normal are not accompanied by significant anomalous easterlies over the eastern Indian Ocean along the Java/Sumatra coast, which is unfavorable for the local Bjerknes feedback and correspondingly for an IOD development. The El Niño/IOD relationship has experienced substantial changes due to the recent decadal El Niño regime shift, which has important implications for seasonal prediction.

Corresponding author: Dr. Wenjun Zhang
College of Atmospheric Sciences, Nanjing University of Information Science and Technology, Nanjing 210044, China
E-mail: zhangwj@nuist.edu.cn

1. Introduction

The El Niño-Southern Oscillation (ENSO) is the dominant low-frequency climate phenomenon resulting from coupled ocean-atmosphere interactions in the tropical Pacific [e.g., Philander et al. 1990; Wallace et al. 1998]. Although ENSO originates in the tropical Pacific, its impacts can be detected in remote oceans through the so-called atmospheric bridge mechanism [e.g., Klein et al. 1999; Alexander et al. 2002; Lau and Nath 2003]. Especially during the mature (boreal winter) and decaying phases (boreal spring) of El Niño, a basin-wide sea surface temperature (SST) warming appears in the tropical Indian Ocean (IO) due to the ENSO-induced surface heat flux anomalies [Klein et al. 1999]. In contrast, during the preceding boreal summer and autumn seasons, a dipole structure of SST anomalies tends to occur in the tropical IO, usually described as the Indian Ocean Dipole (IOD) [Saji et al. 1999; Webster et al. 1999]. A positive IOD event features SST cooling along the Java-Sumatra coast and SST warming in the western tropical IO. A positive correlation between the ENSO and IOD during boreal autumn suggests that IOD events are closely related to ENSO (positive and negative IOD events usually co-occurred with El Niño and La Niña events, respectively) [e.g., Allan et al. 2001; Baquero-Bernal et al. 2002; Xie et al. 2002; Annamalai et al. 2003]. However, this argument was challenged by other studies [e.g., Saji et al. 1999; Webster et al. 1999; Saji and Yamagata 2003; Meyers et al. 2007], which argued that the IOD is an independent mode of coupled ocean-atmosphere climate variability in the tropical IO. Although the ENSO/IOD relationship still remains open to debate, observational and modeling results generally suggest that the IOD seems to be a relatively weak natural mode, which can be excited by external forcings such as the ENSO variability [e.g., Li et al. 2003; Scott et al. 2009].

ENSO exhibits a considerable degree of complexity in its zonal SST anomaly structure. The Central-Pacific, or CP El Niño has occurred more frequently in recent decades, which differs considerably from traditional El Niño events (Eastern-Pacific, or EP El Niño) that are characterized by maximum SST anomalies over the eastern equatorial Pacific [e.g., Ashok et al. 2007; Kao and Yu 2009; Kug et al. 2009]. The CP type of El Niño has become more common while the EP El Niño has occurred less frequently since the 1990s [e.g., Yeh et al. 2009; Xiang et al. 2013; Zhang et al. 2014]. Whether the IOD experienced changes along with the El Niño regime shift deserves attention as the IOD can cause substantial climate anomalies over the Asian-Australian monsoon regions [e.g., Saji and Yamagata 2003; Meyers et al. 2007; Cai et al. 2009]. Another study further separated the CP El Niño into two different sub-types based on different SST anomalies over the subtropical northeastern Pacific and argued that these two CP sub-types exhibit different relationships with the IOD [Wang and Wang 2014]. At present, the exact relationship between the IOD and the two types of El Niño (EP and CP) is still not well understood. Here we discuss the different dynamical linkages between these two types of El Niño and the IOD. We conclude that the relationship between EP El Niño events and the IOD is mainly governed by El Niño event amplitude. In contrast, the CP El Niño/IOD relationship is predominantly governed by the zonal location of El Niño SST anomalies.

2. Data and Methods

The tropical Indo-Pacific SST anomalies were analyzed to demonstrate the ENSO/IOD relationship based on the Hadley Centre sea ice and SST dataset [HadISST; Rayner et al., 2003]. The associated atmospheric circulation was investigated using the National Center for Environmental Prediction/National Center for Atmospheric Research reanalysis data [Kalnay et al., 1996]. We also used sea-surface height data from the Simple Ocean Data Assimilation (SODA 2.2.4) reanalysis [Carton et al., 2000]. The anomalies are defined as a departure from the climatological mean of the entire study period (1951-2013) for all datasets, except for the SODA dataset over the period 1951-2010. A 6-120-month Butterworth band-pass filter is applied to each dataset since inter-annual variability is our focus and we wish to remove the effects of intraseasonal variability such as the Madden-Julian Oscillation, as well as variability on multi-decadal time scales. The datasets were analyzed for the boreal autumn season (September-November: SON), when the IOD usually reaches its peak and El Niño is still developing towards its peak.

The EP and CP El Niño indices (EPI and CPI) were calculated based on a simple transformation [Ren and Jin 2011] (also see the auxiliary material) using Niño3 (SST anomalies averaged over 5°S–5°N and 90°–150°W) and Niño4 (SST anomalies averaged over 5°S–5°N and 160°E–150°W) from the Climate Prediction Center (CPC). El Niño events are identified when the EPI or CPI exceeds 0.6 standard deviation during SON (Fig. 1). All these selected events are also identified as El Niño events by the CPC, except for the 1990 warming event, which has been identified as an El Niño by many other studies [e.g., Ashok et al., 2007; Kug et al. 2009]. Furthermore, the El Niño events with EPI significantly greater than CPI are considered as EP El Niño events, while those with EPI significantly less than the CPI are defined as CP El Niño events. Here, "significance" means a clear separation of respective error bars for the two El Niño flavors (Fig. 1). Therefore, there are eight EP El Niño events (1951, 1957, 1965, 1972, 1976, 1979, 1982, 1997) and eight CP El Niño events (1977, 1986, 1990, 1991, 1994, 2002, 2004, 2009), which is mostly consistent with previous studies [e.g., Ashok et al. 2007; Zhang et al., 2011]. The other five years (1963, 1969, 1987, 2003, 2006) are classified as mixed type El Niño events, which will not be discussed in the remainder of the paper considering the uncertainty of the classification. Our qualitative conclusions remain the same if we use other CP El Niño indices, such as the index defined by Ashok et al. (2007).

3. Results

We first examine the El Niño/IOD linkage during boreal autumn (Fig. 2a). Here, the Niño3.4 index (SST anomalies averaged over 5°S–5°N and 120°–170°W) is used to measure El Niño intensity. The IOD intensity is captured by the dipole mode index (DMI, after Saji et al., 1999), which represents the SST anomaly zonal gradient between the western equatorial (10°S–10°N and 50°–70°E) and southeastern equatorial IO (10°S–0° and 90°–110°E). A strong positive correlation (r=0.67) indicates that a positive IOD usually coincides with El Niño events and becomes stronger as the intensity of El Niño increases. However, this relationship appears to be caused by the EP El Niño events rather than the CP El Niño events (Fig. 2a), which is further confirmed when separating El Niño into the two different flavors (Fig. 2b,c). For the EP El Niño events, the correlation coefficient between the EPI and IOD attains value as high as 0.96 (statistically significant at the 99% level even though there are only 8 samples), indicating a nearly perfect linear relationship. In contrast, no significant linear correlation is found for the CP El Niño events (r=0.16).

Previous studies demonstrated that the atmospheric response is very sensitive to the CP El Niño's SST anomaly zonal location due to the climatological basic state of the Western Pacific Ocean [Zhang et al. 2013, 2015]. Inspired by these works, we examine possible effects of CP El Niño's SST anomaly zonal location on the IOD. The longitude of the maximum zonal gradient of the equatorial (5°S–5°N) mean SST anomalies is used to measure the zonal location of the CP El Niño following the definition of Zhang et al. [2013]. This definition captures well the location of anomalous rising motion in the atmosphere west of the warm SST anomaly center. Here we find a strong linear relationship (r=0.93) between the CP zonal location and the IOD intensity, significant at the 99% confidence level. The IOD tends to be weaker as the CP El Niño shifts further westward. We also test if the EP El Niño's zonal location has an impact on the IOD, but we find no robust indication for this (Fig. S1 in the auxiliary material, r=0.17).

As seen above, different El Niño flavors exhibit very different linkages with the IOD: the relationship for EP events depends on the SST anomaly intensity, while the relationship for CP events depends on the SST anomaly zonal location. Next, we use a composite analysis to explore possible physical mechanisms responsible for the varying El Niño/IOD relationship. We can separate the EP El Niño events with respect to their intensity during boreal autumn. We composite 3 strong EP events (SEP: 1972, 1982, 1997) and 5 weak EP events (WEP: 1951, 1957, 1965, 1976, 1979). The SEP event composite exhibits the typical SST anomaly pattern of traditional El Niño events over the tropical Pacific, which is characterized by strong warm SST anomalies in the eastern tropical Pacific and cold SST anomalies in the western tropical Pacific (Fig. 3a). The atmospheric response occurs mainly over the tropical Pacific with strong surface westerly anomalies over the central and eastern Pacific. Simultaneously, the Walker Circulation weakens with anomalous large-scale ascending motion east of the dateline and anomalous descending motion over the Indo-Pacific region near 120°E (Fig. 3c). Associated with the anomalous sinking motion, a strong anomalous divergence is located over the Indo-Pacific region in the lower troposphere. The surface easterly anomalies near Java-Sumatra are effective in enhancing oceanic upwelling and thermocline tilting in the eastern tropical IO, which brings colder subsurface water to the surface and leads to negative SST anomalies. These cold SST anomalies can further enhance the surface easterly anomalies through the positive "Bjerknes feedback" loop, which favors the development and maintenance of the IOD. In comparison, the WEP event composite shows a similar SST anomaly pattern over the tropical Pacific but with a much weaker intensity (Fig. 3b). Thus, we also find that the associated atmospheric response is weaker for the WEP composite (Fig. 3b,d). Over the Indo-Pacific region, we find much weaker sinking motion and surface easterly anomalies over the tropical IO, which are not effective in initiating the IOD.

Similarly, the CP El Niño events are also separated into two groups: eastward CP El Niño events (ECP: 1991, 1994, 2002) and westward CP El Niño events (WCP: 1977, 1986, 1990, 2004, 2009) according to their SST anomaly zonal locations. The SST anomalies associated with the CP El Niño events are confined to the central tropical Pacific (Fig. 4a,b), very different from the EP El Niño (Fig. 3a,b). For the two groups of CP El Niño events, the WCP composite is located about 15 degrees further westward compared to the ECP composite. In agreement, the atmospheric response to the WCP composite is also located further westward compared to the ECP composite (Fig. 4a-d). For example, the surface westerly anomalies appear over the central equatorial Pacific for the ECP events, while they are located over the western and central equatorial Pacific for the WCP events (Fig. 4a, b). For the Walker Circulation, the center of anomalous rising air is located east of the dateline for the ECP events, whereas it is located west of the dateline for the WCP events (Fig. 4c,d). There is no large difference in the location of the anomalous sinking air between the two groups over the equatorial Indo-Pacific region (Fig. 4c,d), however they exhibit different intensities, which seems inconsistent with the observed difference in surface easterly anomalies over the eastern IO (Fig. 4a,b). The zonal wind anomalies are usually located south of the equator over the eastern IO, which is the upwelling-favoring region off Java-Sumatra. To depict the zonal structure more clearly, we show the surface zonal wind anomalies averaged over the southern equatorial IO (0°-10°S) and the equatorial Pacific (5°S-5°N) to examine the associated atmospheric response (Fig. S2 in the auxiliary material). Consistent with the surface wind anomalies in Figure 4a and b, the zonal wind anomaly center is clearly shifted westward for the WCP events over the tropical Pacific in comparison with the ECP events, and a slight westward displacement is found over the IO. However, over the southeastern equatorial IO, significant easterly anomalies occur near the Java-Sumatra coast during the ECP events while insignificant wind anomalies are found in this region during the WCP events. Away from this key upwelling region, the Bjerknes positive feedback mechanism is weak and cannot effectively produce strong negative SST anomalies over the eastern equatorial IO. Thus, the IOD is not well developed for the WCP event composite. In contrast, the ECP associated easterly anomalies are strong off Java-Sumatra, which favors the establishment of a positive IOD.

The atmospheric responses to the WCP and ECP SST anomaly patterns display a large difference in amplitude in addition to the zonal location (Fig. 4 and S2), which may contribute to the differences in the surface wind anomalies over the southeastern IO. The anomalous response associated with the WCP events is only about half the amplitude of that associated with the ECP events. The interesting question that remains to be addressed is why the atmospheric responses exhibit such a large difference in amplitude between the WCP and ECP event composites despite a similar magnitude of SST anomaly forcing. One possible reason is that the negative SST anomalies over the far-western Pacific during the ECP events are stronger than those during the WCP (Fig. 4a,b). The larger SST anomaly gradient could give rise to a stronger local atmospheric response. A previous theoretical study has demonstrated that the growth rate and period of ENSO over the tropical Pacific decreases as the surface wind anomaly center is displaced westward [Cane et al. 1990]. The upwelling Kelvin wave reflected by the upwelling Rossby wave at the western Pacific boundary during El Niño is more effective at returning the anomalous thermocline to its normal state when the center of the anomalous air/sea interaction is located further westward. To confirm this hypothesis, we used the zonal wind anomaly associated with the WCP and ECP to perform a linear regression on the sea-surface height (SSH) anomalies (Fig. S3 in the auxiliary material). Here the regions of 5°S–5°N, 160°–180°E and 5°S–5°N, 150°–170°E are selected as the key areas of anomalous westerly activity for the ECP and WCP events, respectively, according to their surface wind anomaly patterns (Fig. 4a,b). We see that the zonal gradient of the anomalous SSH for the WCP-related surface westerly anomalies is weaker than that for the ECP. Especially over the western Pacific, the negative equatorial-mean SSH anomalies are much stronger for the ECP associated surface westerly anomalies than those for the WCP. The stronger IOD for the ECP events also contributes to a stronger Walker Circulation response and thus stronger divergence anomalies over the Indo-Pacific region and zonal surface wind anomalies compared to WCP events. Additionally, it is notable that stronger negative cloud-radiation feedback could also play a certain role on the weaker atmospheric response during the WCP than that during the ECP, due to a different background SST pattern.

4. Conclusions and Discussion

A large positive correlation (r=0.67) is found between the intensity of the El Niño and IOD phenomena during the boreal autumn season for 1951-2013. However, this linkage is attributed to Eastern-Pacific (EP) El Niño events rather than Central-Pacific (CP) El Niño events. Considering different El Niño flavors, their relationships with the IOD exhibit very different characteristics. For the EP El Niño type, a near perfect linear correlation (r=0.96) is detected between the El Niño intensity and the simultaneous IOD intensity. Compared to the strong EP (SEP) events, the weak EP (WEP) events are usually accompanied by a weaker atmospheric response and thus weaker surface easterly anomalies over the eastern IO. These weak easterly anomalies are not able to induce a strong local air-sea interaction and thus are not efficient in causing an IOD event. However, the zonal location of CP El Niño events is highly correlated with the IOD intensity (r=0.93). Along with the westward movement of the westward CP (WCP) compared to the eastward CP (ECP), the associated atmospheric anomalies are shifted westward over the tropical Pacific as well. Over the upwelling-favoring region off Java-Sumatra, significant easterly anomalies occur during the ECP events while insignificant wind anomalies are found during the WCP events. Thus, the Bjerknes positive feedback in the IO cannot effectively be perturbed during the WCP, resulting in only a weak IOD. It can be seen that the El Niño/IOD relationship experienced a remarkable change due to the ENSO regime shift. Especially for recent decades when the CP type dominates the El Niño phenomenon, the zonal location of El Niño events need be emphasized to examine the

ENSO/IOD relationship.

A previous study [Wang and Wang, 2014] further separated the CP El Niño into two sub-types and argued, based on composite analysis that one sub-CP type co-occurs with positive phases of the IOD while the other sub-CP type accompanies negative phases of the IOD. However, no negative values of the DMI (and thus no negative IOD events) are found in this study (Fig. 2d). The difference between their and our results can be explained by the choice of selected El Niño events and the differing methodologies. For instance, the CP region exhibits pronounced decadal variability [Zhang et al. 2014], which we remove in our study, as the interaction between the interannual ENSO phenomenon and the IOD is our focus. It is also noted that they used normalized IOD values, while raw values are used here. We emphasize the importance of considering the zonal location of the El Niño events in addition to its amplitude when assessing the interaction of El Niño with the tropical Indian Ocean.

Another previous study displayed a high consistency between ENSO amplitude and the ENSO/IOD correlation, especially exhibiting a simultaneous decadal enhancement around the late 1970s [Santoso et al. 2012], which is consistent with the EPI/IOD relationship in this study. However, this consistency may be weakened due to more frequent occurrences of CP El Niño events in the recent decade. This study also sets a further challenge for forecast models to accurately predict both the amplitude and location of El Niño – our earlier work suggests that impactful teleconnections greatly depend on whether a CP or EP El Niño occurs [e.g., Zhang et al., 2014] – but here we go further to suggest that the location of the CP events themselves causes a great variation in connections to the Indian Ocean. Further efforts are thus required to more realistically capture different El Niño features in coupled climate models although considerable process has been made [e.g., Guilyardi et al. 2009; Bellenger et al. 2014].

Acknowledgements The data used to reproduce the results of this paper are available for free by contacting the corresponding author. This work is supported by the Special Fund for Public Welfare Industry (Meteorology) (GYHY201506013, GYHY201406022), the National Basic Research Program "973" (Grant No. 2012CB417403), and Jiangsu Provincial Qinglan Project.

References

Alexander, M. A., I. Blade, M. Newman, J. R. Lanzante, N.-C. Lau, and J. D. Scott (2002), The atmospheric bridge: The influence of ENSO teleconnections on air-sea interaction over the global oceans, *J. Clim.*, 15, 2205–2231.

Allan, R. J., et al. (2001), Is there an Indian Ocean Dipole independent of the El Niño-Southern Oscillations? *CLIVAR Exch.*, 6(3), 18–22.

Annamalai, H., R. Murtugudde, J. Potemra, S.-P. Xie, P. Liu, and B. Wang (2003), Coupled dynamics over the Indian Ocean: Spring initiation of the zonal mode, *Deep Sea Res.*, Part II, 50, 2305–2330.

Ashok, K., S. K. Behera, S. A. Rao, H. Y. Weng, and T. Yamagata (2007), El Niño Modoki and its possible teleconnection, *J. Geophys. Res.*, 112, C11007, doi:10.1029/2006JC003798.

Baquero-Bernal, A., M. Latif, and S. Legutke (2002), On dipolelike variability of sea surface temperature in the tropical Indian Ocean, *J. Clim.*, 15, 1358–1368.

Bellenger, H., E. Guilyardi, J. Leloup, M. Lengaigne, J. Vialard (2014), ENSO representation in climate models: from CMIP3 to CMIP5, Clim. Dyn., 42, 1999–2018.

Cai W., T. Cowan, and A. Sullivan (2009), Recent unprecedented skewness towards positive Indian Ocean dipole occurrences and its impact on Australian rainfall, *Geophys. Res. Lett.*, 36, L11705, doi:10.1029/2009GL037604.

Cane, A. M., M. Munnich, and S. E. Zebiak (1990), A study of self-excited oscillation of the tropical ocean-atmosphere systems. PartI: Linear analysis. *J. Atmos. Sci.*, 47, 1562–1577.

Carton, J. A., G. Chepurin, X. Cao, and B. Giese (2000), A simple ocean data assimilation analysis of the global upper ocean 1950–95. Part I: Methodology, *J. Phys. Oceanogr.*, 30, 294–309.

Guilyardi, E., A. Wittenberg, A. Fedorov, M. Collins, C. Wang, A. Capotondi, G. J. van Oldenborgh, and T. Stockdale (2009), Understanding El Niño in ocean–atmosphere general circulation models: Progress and challenges, *Bull. Amer. Meteor. Soc.*, 90, 325–340.

Kalnay, E., and Coauthors (1996), The NCEP/NCAR 40-year reanalysis project, *Bull. Am. Meteorol Soc.*, **77**, 437– 471.

Kao, H. Y., and J. Y. Yu (2009), Contrasting eastern-Pacific and central-Pacific types of ENSO, *J. Clim.*, 22, 615–632.

Klein, S. A., B. J. Soden, and N.-C. Lau (1999), Remote sea surface temperature variations during ENSO: Evidence for a tropical atmospheric bridge, *J. Clim.*, 12, 917–932.

Kug, J.-S., F.-F. Jin, and S.-I. An (2009), Two types of El Niño events: Cold tongue El Niño and warm pool El Niño, *J. Clim.*, 22, 1499–1515.

Lau, N.-C., and M. J. Nath (2003), Atmosphere-ocean variations in the Indo-Pacific sector during ENSO episodes, *J. Clim.*, 16, 3–20.

Li, T., B. Wang, C.-P. Chang, and Y. Zhang (2003), A theory for the Indian Ocean Dipole-Zonal Mode, *J. Atmos. Sci.*, 60, 2119–2135.

Meyers, G., P. McIntosh, L. Pigot, and M. Pook (2007), The years of El Niño, La Niña, and interactions with the tropical Indian Ocean, *J. Clim.*, 20, 2872–2880.

Philander SG (1990), El Niño, La Niña, and the Southern Oscillation, Academic, San Diego.

Rayner, N. A., D. E. Parker, E. B. Horton, C. K. Folland, L. V. Alexander, D. P. Rowell, E. C. Kent, and A. Kaplan (2003), Global analyses of sea surface temperature, sea ice, and night marine air temperature since the late nineteenth century, *J. Geophys. Res.*, 108, 4407, doi:10.1029/2002JD002670.

Ren, H.-L., and F.-F. Jin (2011), Niño indices for two types of ENSO, *Geophys. Res. Lett.*, 38, L04704, doi:10.1029/2010GL046031.

Saji, N. H., and T. Yamagata (2003), Structure of SST and surface wind variability during Indian Ocean Dipole mode events: COADS observations, *J. Clim.*, 16, 2735–2751.

Saji, N. H., B. N. Goswami, P. N. Vinayachandran, and T. Yamagata (1999), A dipole in the tropical Indian Ocean, *Nature*, 401, 360–363.

Santoso, A., M. H. England, and W. Cai (2012), Impact of Indo-Pacific feedback interactions on ENSO dynamics diagnosed using ensemble climate simulations, *J. Clim.*, 25, 7743–7763.

Scott, A. F., S.-P. Xiang, and J. P. McCreary Jr. (2009), Indian Ocean circulation and climate variability, *Rev. Geophys.*, 47, doi:10.1029/2007RG000245.

Wallace, J. M., E. M. Rasmusson, T. P. Mitchell, V. E. Kousky, E. S. Sarachik, and H. Von Storch (1998), On the structure and evolution of ENSO-related climate variability in the tropical Pacific: Lessons from TOGA, *J. Geophys. Res.*, 103, 14241–14259.

Wang, X., and C. Wang (2014), Different impacts of various El Niño events on the Indian Ocean Dipole, *Clim. Dyn.*, 42, 991–1005.

Webster, P. J., A. M. Moore, J. P. Loschnigg, and R. R. Leben (1999), Coupled oceanic-atmospheric dynamics in the Indian Ocean during 1997–98, *Nature*, 401, 356–360.

Xiang, B., B. Wang, T. Li (2013), A new paradigm for predominance of standing

Central Pacific Warming after the late 1990s, *Clim. Dyn.*, 41, 327–340.

Xie, S.-P., H. Annamalai, F. A. Schott, and J. P. McCreary (2002), Structure and mechanisms of south Indian Ocean climate variability, *J. Climate*, 15, 867–878.

Yeh, S. W., J. S. Kug, B. Dewitte, M. H. Kwon, B. P. Kirtman, and F.-F. Jin (2009), El Niño in a changing climate, *Nature*, 461, 511–514.

Zhang, W., F.-F. Jin, and A. Turner (2014), Increasing autumn drought over southern China associated with ENSO regime shift, *Geophys. Res. Lett.*, 41, doi:10.1002/2014GL060130.

Zhang, W., F.-F. Jin, J. Li, and H.-L. Ren (2011), Contrasting impacts of two-type El Niño over the western North Pacific during boreal autumn, *J. Meteorol. Soc. Jpn.*, 89, 563–569.

Zhang, W., F.-F. Jin, J. X. Zhao, L. Qi and H.-L. Ren (2013), The possible influence of a non-conventional El Nino on the severe autumn drought of 2009 in Southwest China, *J. Clim.*, 26, 8392–8405.

Zhang, W., H. Li, F.-F. Jin, M. F. Stuecker, A. G. Turner, and N. P. Klingaman (2015), The annual-cycle modulation of meridional asymmetry in ENSO's atmospheric response and its dependence on ENSO zonal structure, *J. Clim.*, 28, 5795–5812.

Figure Captions

Figure 1. Normalized EPI (red) and CPI (green) during all El Niño boreal autumn (SON) seasons for the 1951-2013 period (note that El Niño events only are shown, not all years). Error bars represent 0.5-standard deviation error estimates for EPI and CPI. EP and CP indicate different types of El Niño as described in the text. MIX denotes mixed El Niño events that cannot be clearly separated into the two types. Units are □.

Figure 2. Scatter diagrams of DMI (□) with (a) the Niño3.4 (□) for both EP (circle) and CP (square) El Niño events, (b) the intensity (EPI in □) of EP El Niño events, (c) the intensity (CPI in □) of CP El Niño events, and (d) longitude (Xt; °E) of CP El Niño events during autumn. The longitudinal position is defined as the longitude of

the maximum zonal gradient of the equatorial (5°S–5°N) mean SST anomalies. The correlation coefficients in (a), (b), and (d) exceeds the 99% confidence level, while correlation coefficient in (c) is not statistically significant at the 80% confidence level.

Figure 3. Composite SST (shading in □) and surface wind (vector in m/s) anomalies for strong (a) and weak (b) El Niño events; (c) and (d) are the same as the (a) and (b) except for the anomalous vertical pressure velocity (shading in 10^{-2} Pa s^{-1}), Walker Circulation (vector in m s^{-1}; the anomalous vertical velocity being multiplied by a factor of -100), and velocity potential (contour in 10^{6} m^{2} s^{-1}) averaged over 5°S–5°N. The shading and vector are only shown when the values are significant at the 90% significance level from a two-tailed Student t-test.

Figure 4. Same as Figure 3, but for the East and West CP El Niño event composite. The green dot in (a) and (b) marks the zonal location of the East and West El Niño event composite (based on the maximum zonal SSTA gradient), respectively.

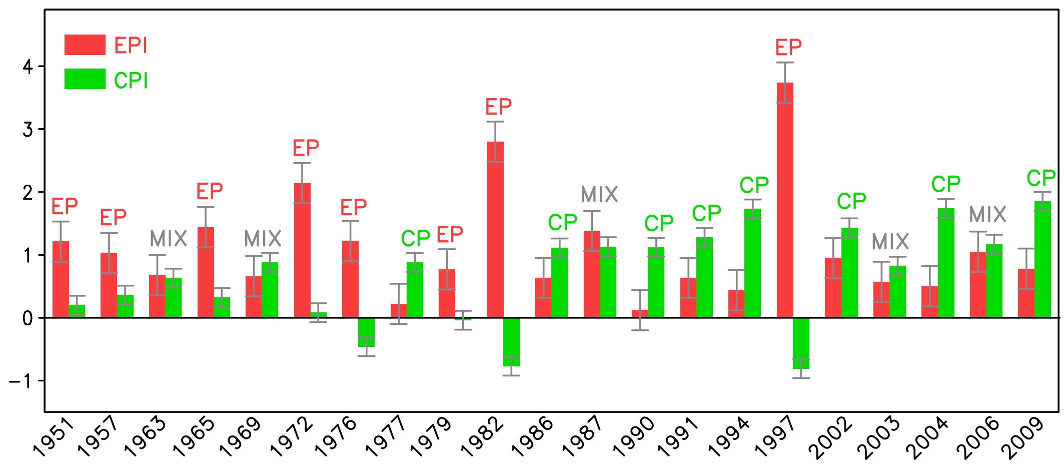

EPI
CPI
4
3
2
1
0
−1
EP
EP
MIX
EP
MIX
EP
EP
CP
EP
EP
CP
MIX
CP
CP
CP
EP
CP
MIX
CP
MIX
CP
1951
1957
1963
1965
1969
1972
1976
1977
1979
1982
1986
1987
1990
1991
1994
1997
2002
2003
2004
2006
2009

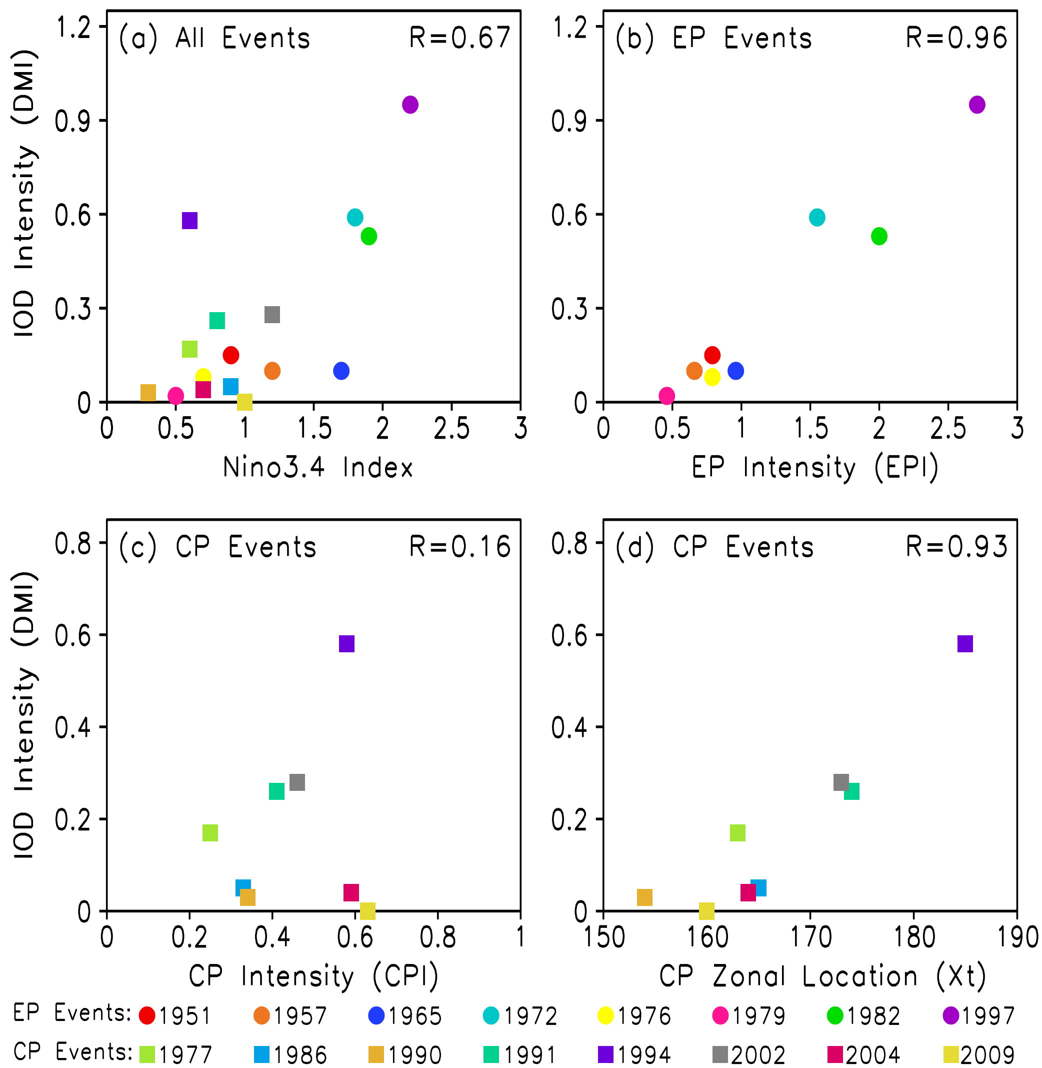

(a) All Events
R=0.67
(b) EP Events
R=0.96
(c) CP Events
R=0.16
(d) CP Events
R=0.93
IOD Intensity (DMI)
Nino3.4 Index
EP Intensity (EPI)
CP Intensity (CPI)
CP Zonal Location (Xt)
EP Events: 1951 1957 1965 1972 1976 1979 1982 1997
CP Events: 1977 1986 1990 1991 1994 2002 2004 2009

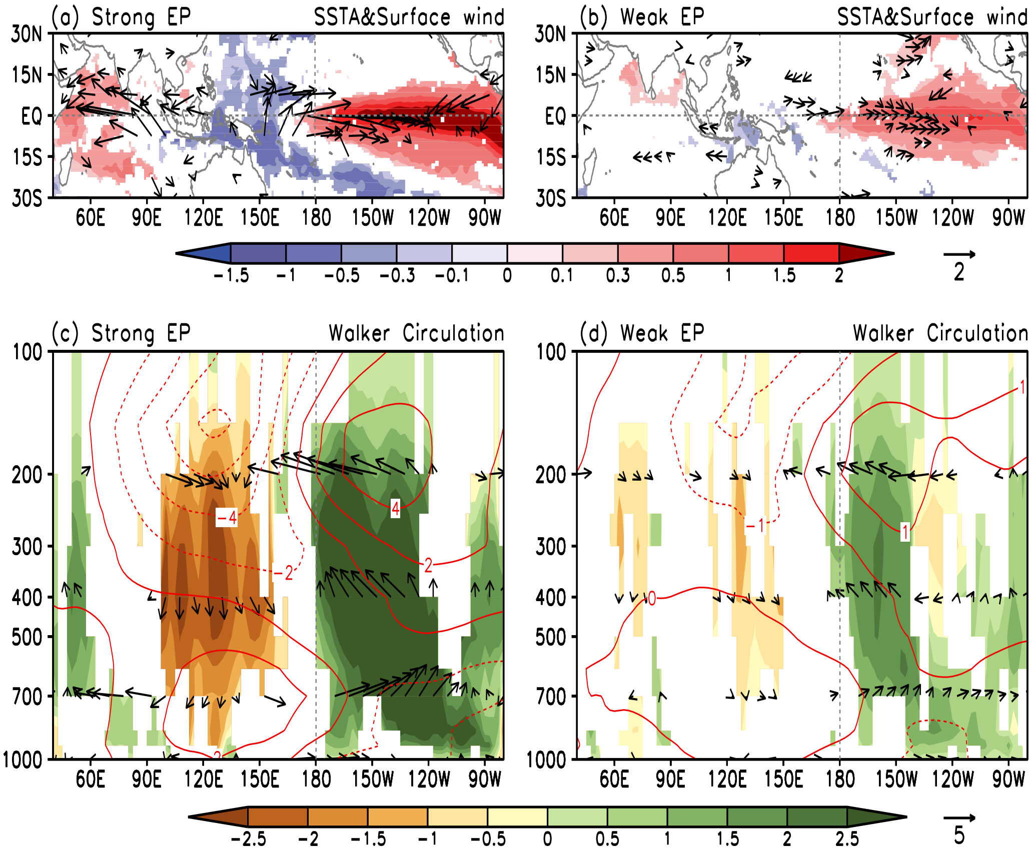

(a) Strong EP
SSTA&Surface wind
(b) Weak EP
SSTA&Surface wind
30N
15N
EQ
15S
30S
60E 90E 120E 150E 180 150W 120W 90W
−1.5 −1 −0.5 −0.3 −0.1 0 0.1 0.3 0.5 1 1.5 2
2
(c) Strong EP
Walker Circulation
(d) Weak EP
Walker Circulation
100
200
300
400
500
700
1000
−2.5 −2 −1.5 −1 −0.5 0 0.5 1 1.5 2 2.5
5

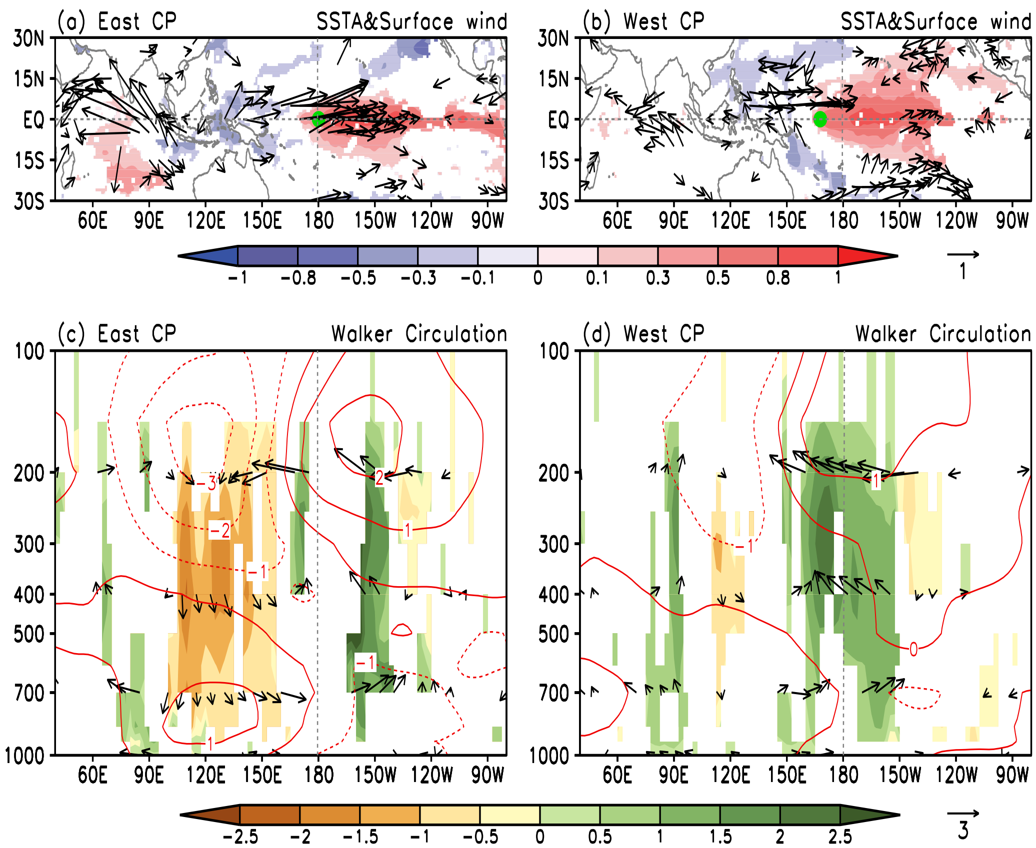

(a) East CP
SSTA&Surface wind
(b) West CP
SSTA&Surface wind
30N
15N
EQ
15S
30S
60E 90E 120E 150E 180 150W 120W 90W
-1 -0.8 -0.5 -0.3 -0.1 0 0.1 0.3 0.5 0.8 1
1
(c) East CP
Walker Circulation
(d) West CP
Walker Circulation
100
200
300
400
500
700
1000
-2.5 -2 -1.5 -1 -0.5 0 0.5 1 1.5 2 2.5
3